South Dakota State University

Open PRAIRIE: Open Public Research Access Institutional Repository and Information Exchange

Mechanical Engineering Engineering Faculty Publications

Department of Mechanical Engineering

2009

Initial Fixation of a Femoral Knee Component: An In vitro and Finite Element Study

Travis A. Burgers
University of Wisconsin-Madison, travis.burgers@sdstate.edu

Jim Mason

Heidi-Lynn Ploeg
University of Wisconsin-Madison

Follow this and additional works at: https://openprairie.sdstate.edu/me_pubs

Recommended Citation

Burgers, Travis A.; Mason, Jim; and Ploeg, Heidi-Lynn, "Initial Fixation of a Femoral Knee Component: An In vitro and Finite Element Study" (2009). *Mechanical Engineering Engineering Faculty Publications*. 5.
https://openprairie.sdstate.edu/me_pubs/5

This Article is brought to you for free and open access by the Department of Mechanical Engineering at Open PRAIRIE: Open Public Research Access Institutional Repository and Information Exchange. It has been accepted for inclusion in Mechanical Engineering Engineering Faculty Publications by an authorized administrator of Open PRAIRIE: Open Public Research Access Institutional Repository and Information Exchange. For more information, please contact michael.biondo@sdstate.edu.

Initial Fixation of a Femoral Knee Component: An *In Vitro* and Finite Element Study

Travis A. Burgers[1], Jim Mason[2], Heidi-Lynn Ploeg[3,*]

1. Department of Mechanical Engineering, University of Wisconsin-Madison, 1513 University Avenue, Madison, WI 53706-1572, email: tburgers@wisc.edu
2. Zimmer, Inc., PO Box 708, MS 1901, Warsaw, IN 46581-0708, email: jim.mason@zimmer.com
3. Department of Mechanical Engineering and Biomedical Engineering, University of Wisconsin-Madison, 1513 University Avenue, Madison, WI 53706-1572, email: ploeg@engr.wisc.edu

* Corresponding author

Abstract: Loosening is the primary cause of total knee arthroplasty implant failure; therefore, to investigate this failure mode femoral knee components were implanted *in vitro* on three cadaveric femurs. Bone-implant finite element (FE) models were created to predict the initial fixation of the interface of each femur. Initial fixation of the femoral knee component was successfully measured with the strain gauged implants. Subject-specific FE models were calibrated using the *in vitro* strain measurements and used to assess initial fixation. Initial fixation was shown to increase with bone density. The geometry of the implant causes the distal femur to deform plastically. It also causes higher stresses in the lateral side and higher pressures on the lateral surfaces. The implementation of plasticity in the bone material model in the FE model decreased these strains and pressures considerably from a purely elastic model, which demonstrated the importance of including plasticity.

Keywords: distal femur, femoral knee components, initial fixation, implant loosening, *in vitro* testing, finite element analysis, press-fit, cementless, biomechanics, experimental, computational

Biographical Notes: Travis Burgers is a PhD candidate in Mechanical Engineering at the University of Wisconsin-Madison. In his dissertation project, he is assessing the fixation strength of femoral knee components using in vitro cadaveric experiments and patient-specific finite element models. He earned a BSE degree with an emphasis in Mechanical

Copyright © 200x Inderscience Enterprises Ltd.

Engineering from Dordt College and a MS degree in Civil Engineering with an emphasis in structural engineering from Colorado State University.

Dr. Jim Mason is the Associate Director of Research in the Trauma Division at Zimmer, Inc. Formerly he was the Director of the Biomechanics Research Laboratory and an associate professor in the Department of Aerospace and Mechanical Engineering at the University of Notre Dame.

Dr. Heidi-Lynn Ploeg is an Assistant Professor in Mechanical and Biomedical Engineering at the University of Wisconsin-Madison. Her career objective is to understand the human musculo-skeletal system better, in order to aid the development of biomechanical and safe solutions for the care and treatment of diseased or injured systems. Her research interests include studying the nature of bone, bone growth, and joint biomechanics as they relate to the orthopaedics industry as well as to the developing field of computer-aided surgery. She is engaged in research involving traditional mechanical testing methods and finite-element analysis.

---

1 Introduction

Implant survival rates are a primary concern for individuals receiving a primary total knee arthroplasty (TKA). The most common mode of TKA failure is loosening, which is the cause of 44% of TKA revision surgeries (Robertsson et al., 2001). A number of authors have reported the failure rates of TKA femoral components. King and Scott reported that 1% of 1600 TKA surgeries failed due to femoral loosening at seven years but did not report the type of fixation (King and Scott, 1985). Haas et al. reported 33% of 76 knees required a revision TKA due to a loose femoral component (Haas et al., 1995). Chockalingam and Scott performed survival and radiographic analyses on 352 patients and found there was a 9.8% and 0.6% aseptic loosening rate of cementless and cemented femoral components at six years, respectively (Chockalingam and Scott, 2000). TKAs are relatively successful compared to other types of surgeries (Sharkey et al., 2002), but due to the large number of TKAs (over 500,000 annually in both the US (DeFrances et al., 2007) and Europe (Europe Information Society, 2007)), even a small percentage of failures leads to a large number of revisions (King and Scott, 1985).

It is recognized that one cause for aseptic loosening is a lack of initial post-operative (primary) fixation (Maloney et al., 1989, Phillips et al., 1990, Viceconti et al., 2000). Finite element (FE) analysis has been used to investigate the fixation of cementless components such as an acetabular component (Udofia et al., 2007) and a femoral hip component (Reggiani et al., 2007). FE models of femoral knee components have been created to investigate stress shielding in the bone due to the components (Tissakht et al., 1996, van Lenthe et al., 1997, Barink et al., 2003), bone remodeling in primary and stemmed revision components (van Lenthe et al., 2002) and the viscoelastic response of cortical bone around a stemmed revision component (Shultz et al., 2006). Completo et al. validated FE models of femoral knee components on synthetic femurs by experimentally measuring cortex bone strains under physiological loading conditions (Completo et al., 2007). FE models of the femoral component have not yet been used to investigate the initial fixation of cementless, stemless primary femoral knee components. Thus, the goals of this study were first, to measure the *in vitro* fixation characteristics of the press-fit femoral knee component by surgically implanting the knee component on three cadaveric femurs; and, second, to create accurate FE models from computed tomography (CT) scan data of the cadaveric femurs used in the experiment and validate the models by comparing the results to *in vitro* measures.

2 Methods

In this study femoral knee components were implanted *in vitro* on three cadaveric femurs. Bone-implant FE models were created to predict the fixation strength of the interface of each femur. In addition to the bone-implant FE models, FE models of only the implant with porous coating were created and validated against experimental testing of strain gauged implants.

2.1 In vitro Implantation

Three left human cadaveric femurs were obtained from a major regional university through the Uniform Anatomical Gift Act. The femurs were received with the soft tissue removed. Each had been wrapped in saline-saturated gauze, sealed in an airtight plastic bag and frozen to -20 °C. Radiographic analysis showed that two femurs had normal bone density and the other had low bone density. The femurs used are listed in Table 1

with the corresponding implant and relative density rank among the three bones used.

Table 1 Relative Density Ranking of Femurs used for *In Vitro* Experiment

Bone ID	Density	Relative density rank	Implant
F-1	Normal bone density	1	NexGen size F
D-1	Normal bone density	2	NexGen size D
D-2	Low bone density	3	NexGen size D

The NexGen® Complete Knee Solution (Zimmer, Inc., Warsaw, IN) cementless femoral knee component was chosen for this study. Figure 1 shows a photograph of the implanted component on the femur with the anterior shield, posterior condyles and implant box region labeled. Initial fixation for this implant is caused by a press-fit. The bone is surgically cut so that the anterior-posterior (AP) dimension of the femur is larger than that of the box by 3-4 mm. Upon implantation the bone compresses in the AP direction to fit inside the implant. This causes a press-fit force between the bone and the implant. This force also causes the implant to deform, primarily with the shield and condyles bending outward in the sagittal plane.

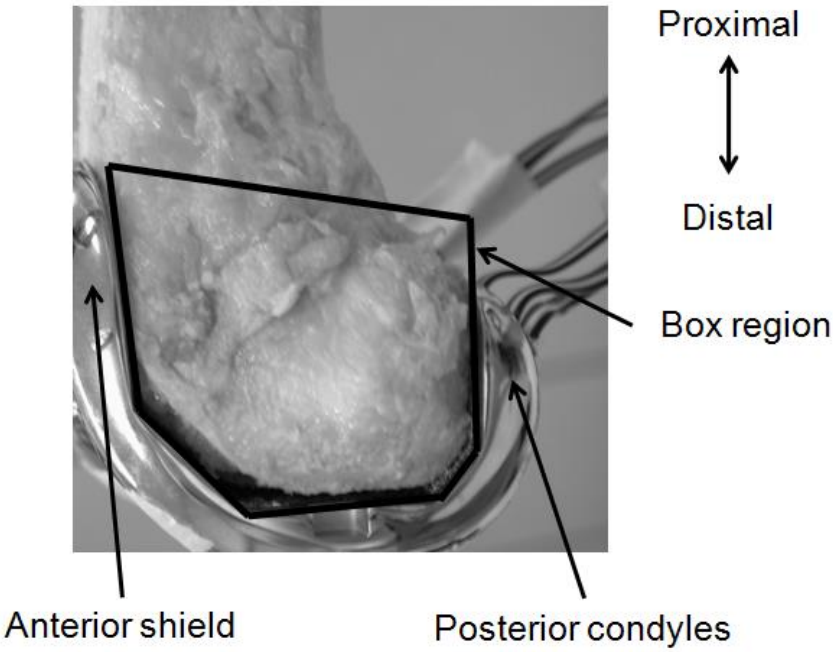

Figure 1 Sagittal View of Implanted Femoral Knee Component. The anterior shield, posterior condyles and implant box region are labeled.

Four triaxial strain gauge rosettes (CEA-06-062UR-250, Measurements Group Inc., Raleigh, NC) were bonded to each of the implants. Two strain rosettes were attached to the anterior shield and one on each posterior condyle (Figure 2). Due to the press-fit with the flange and condyles bending outward, the primary strains on the external face are compressive strains. Thus the magnitude of the minimum principal strain is expected to be larger than that of the maximum principal strain. The specific locations were chosen based on the results of a preliminary FE analysis of the implants. The locations were restricted to surfaces which would not be in contact with the bone or be impacted during the implantation procedure. In the preliminary FE models, a unit pressure was applied to the interior anterior shield and posterior condyles while the interior distal faces were fixed (Figure 3). The four strain rosette locations were chosen in regions with a relatively high strain and low strain gradient.

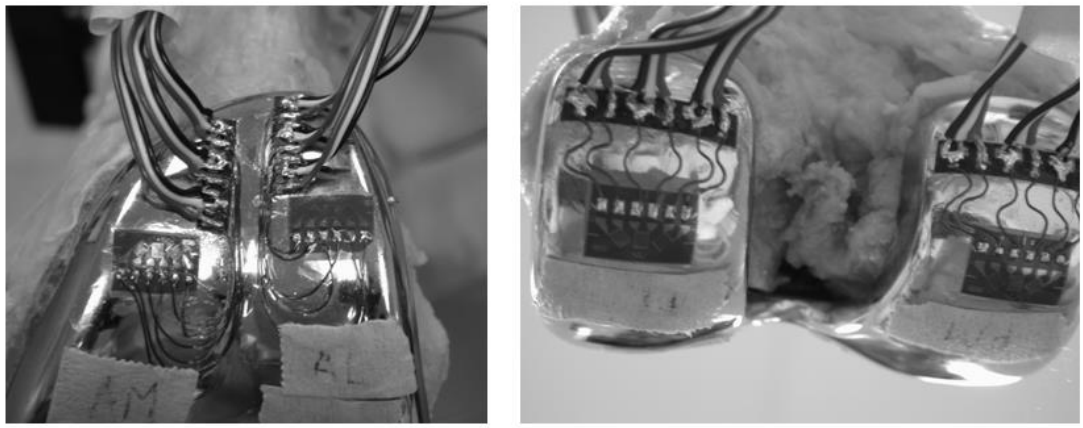

a b

Figure 2 Photographs of Strain Rosette Locations. a) Anterior view showing rosettes on anterior shield, b) Posterior view showing rosettes on each posterior condyle.

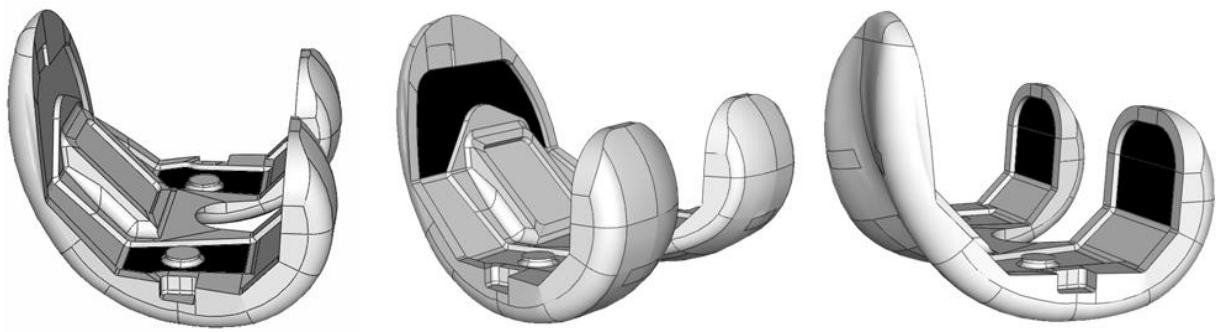

a b c

Figure 3 Preliminary FE Model Boundary Conditions. a) Interior distal faces shown in black were fixed, b) Unit pressure was applied at interior anterior shield face shown in black, c) Unit pressure was applied at interior posterior condyle faces shown in black.

Surgical cuts were made on each femur according to the manufacturer's surgical technique and the implant size for each bone was determined (Table 1). The femurs were thawed at room temperature for a minimum of six hours and the femoral knee components were implanted onto the bones using surgical tools and methods. Strains in each rosette were measured at a sampling rate of 100 Hz for one second before and immediately after implantation. A 5 Hz low pass filter was used to reduce the signal noise. The mean and standard deviation of the filtered data were calculated and

used to find the principal strains for each strain rosette. The difference between the pre- and post-implantation strains was calculated and compared.

2.2 Implant Experimental Testing for FE Model Validation

A NexGen implant was subjected to mechanical testing so that the FE model of the implant with its porous coating could be validated. The implant used in the validation testing was the same strain gauged component that was implanted on the F-1 bone in the *in vitro* test. A device was designed and constructed to fix the implant and apply a load to the anterior shield of the implant representative of a press-fit condition on the anterior face. This device is shown in Figure 4 and was composed of a fixation flange, an angled insert and a yoke. The angled insert was designed to fix the implant at a 5° angle, the same angle as between the distal interior face of the implant and the interior anterior shield in the sagittal plane. The insert fixed the implant so that the load was applied perpendicular to the anterior shield.

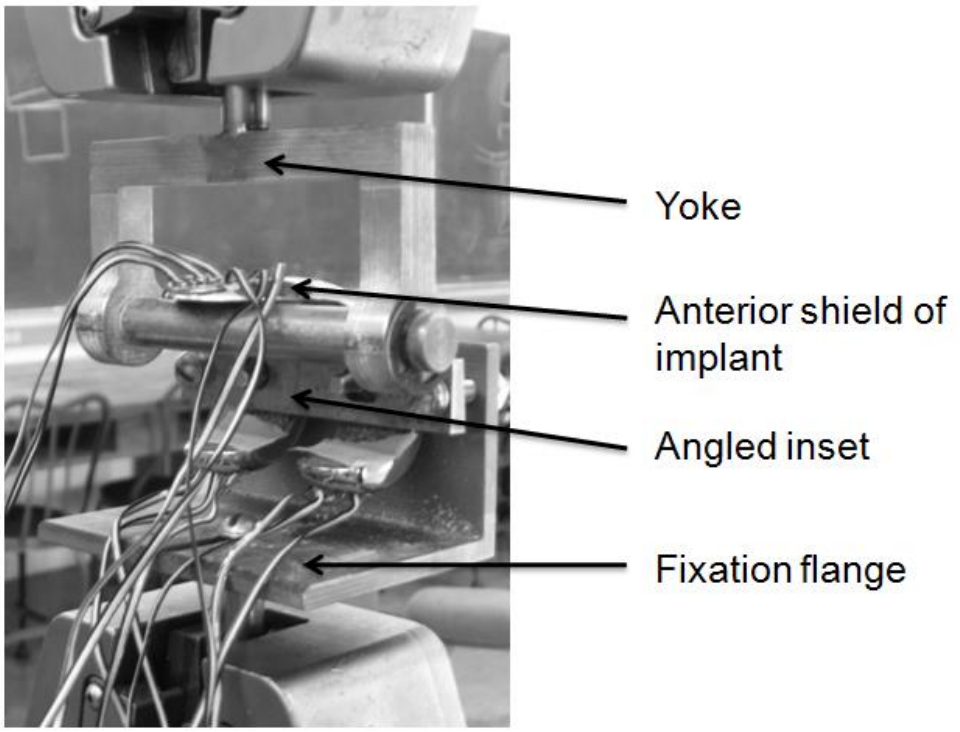

Figure 4 Photograph of the Test Setup for the F-1 Implant Validation Test.

The fixation flange and yoke each had 13 mm (0.50 inch) diameter cylinders which were fixed in the grips of an MTS Sintech 10GL screw driven load frame. A 50 kN MTS 643 load cell (MTS Systems Corporation, Eden Prairie, MN) was attached to the frame. The yoke was displaced so that the load was applied at 30 N/second (7 lbs/second) to simulate a quasi-static loading condition. The load was cycled between 110 and 890 N (25 - 200 lbs) ten times to precondition the implant. Then an 890 N load was applied and strain was measured in the anterior gauges using a strain gauge conditioner and data acquisition system. A three-wire quarter Wheatstone bridge circuit was used to measure the strain in each gauge. This bridge configuration automatically compensated for temperature effects. Principal strains were calculated for each rosette.

The point of load application between the yoke and the anterior shield was documented. A piece of masking tape was attached to the porous coating during testing. The yoke was sprayed with Spotcheck® (Magnaflux, Glenview, IL), a penetrant film used to identify surface cracks. Figure 5 shows the white line on the masking tape left from the Spotcheck® film where the yoke contacted the porous coating. The width and height of the load application area were measured. This area was located with respect to the edge of the porous coating. These measurements were recorded so that the load application location could be reproduced in the FE model of the experiment.

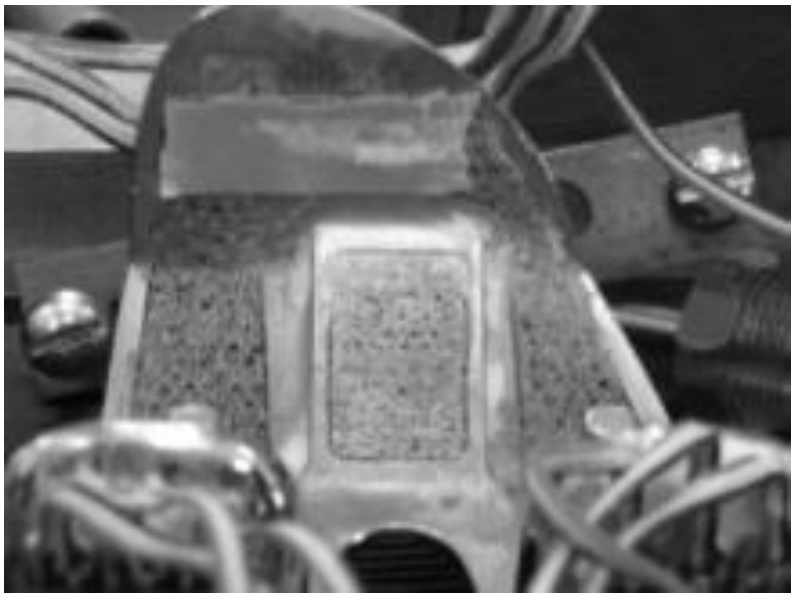

Figure 5 Photograph of the Posterior View of the Interior Side of Implant. The load application region was determined from Spotcheck® on masking tape.

2.3 Validation of the Finite Element Model of the Implant

A finite element model of the implant experimental testing described above was created. The computer-aided design (CAD) model of the geometry of the implant and the yoke were imported into Abaqus 6.7-1 (Simulia, Providence, RI), . The implant pegs were removed to simplify the geometry since they were assumed to have a negligible effect on the structural stiffness of the implant and the initial press-fit fixation. The material properties of the metals were defined as shown in Table 2. All the metals used in the models were assumed to be linear elastic, homogeneous and isotropic. The implant material was a cobalt chrome alloy (CoCr) with a titanium (Ti) porous coating. The material of the yoke was low alloy steel.

Table 2 Mechanical Properties of Metals in the FE Model.

Material	Modulus of Elasticity (MPa)	Poisson's ratio

CoCr	210,000 (van Lenthe et al., 2002, Shultz et al., 2006, Completo et al., 2007)	0.3
Ti porous coating	6900	0.3
Steel	200,000	0.3

Nodes on the common surface of the CoCr-Ti interface were "tied," therefore constraining the degrees of freedom of the nodes on the Ti porous coating surface to have exactly the same displacements and rotations as the coincident nodes on the CoCr surface.

A node-to-surface, small sliding penalty formulation was used to define the contact conditions in the normal direction of the yoke-Ti porous coating interface. Frictional contact was defined between the yoke and the Ti coating using a penalty friction formulation with a static coefficient of friction of 0.5. The load application area was modeled following the measurements from the validation experiment.

Strain rosette locations were determined by digitizing their location on the implants using a Shape Grabber SG100 laser scanner (Shape Grabber, Inc., Ottawa, Ontario) with a resolution of 0.1 mm. According to these measurements, a 4 mm by 10 mm region was defined at these locations in the FE model. The implant was meshed with quadratic tetrahedral elements. A mesh convergence test was performed on the implant mesh using principal strains in the locations of the strain rosettes. Based on the results of the mesh convergence test, a global mesh size of 1.5 mm was used with a local size of 0.8 mm in the strain rosette locations.

A load of 890 N was applied to the cylindrical end of the yoke normal to the interior anterior face of the implant as shown in Figure 6. Displacements at the interior distal faces were fixed (as in Figure 3) to represent the fixation locations during the experiment. Principal strains were calculated at each node and averaged over each anterior strain rosette location.

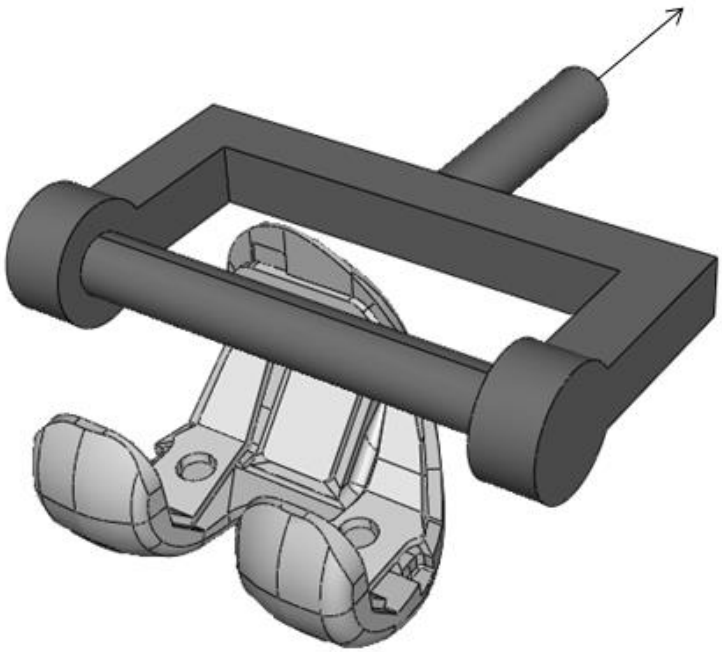

Figure 6 Diagram of Load Applied through Yoke. This was used in the FE model to validate the implant.

2.4 Bone-Implant Finite Element Models

To investigate the mechanics of the bone-implant press-fit, finite element models of the bone and implant composite were created. The geometry of each bone was recreated from transverse CT scans of the cadaveric femurs used in the *in vitro* implantation previously described. The bones were prepared for implantation with the appropriate surgical cuts and CT scanned using a GE Litespeed CT scanner (Madison, WI) with a slice thickness and spacing of 0.625 mm. The CT data was processed to create a FE mesh with the following steps: first, the CT data was segmented (Mimics 10, Materialise, Ann Arbor, MI); second, a nonuniform rational B-spline (NURBS) surface was created and smoothed (Geomagic Studio 8, Raindrop Geomagic, NC); third, the solid model was prepared and edited (Unigraphics 4, EDS, Plano, TX); and, fourth, the FE mesh was prepared for FE analysis (Abaqus 6.7-1, Simulia, Providence, RI). Only the distal 70 mm of the femur was modeled since it was assumed that the rest of the femur would have a negligible influence on the press-fit interaction.

The properties of the metals were the same as those used in the implant FE model described above. Bone was assumed to be heterogeneous and isotropic using properties in the AP direction, since the loading in this application is primarily in the AP direction. Apparent density was derived from CT density using the linear relation in

(1 (Rho et al., 1995). In this equation *HU* is the CT number in Hounsfield units and apparent density, ρ_{app}, is in g/cm^3. The AP modulus of elasticity was related to apparent density using the power-law relation in (2 (Rho et al., 1995). In this equation the modulus of elasticity, *E*, is in MPa and apparent density, ρ_{app}, is in g/cm^3.

$$\rho_{app} = 0.00121\ HU + 0.139 \quad (1)$$

$$E = 3280\ \rho_{app}^{1.79} \quad (2)$$

The mechanical properties of the bone were assigned to the mesh on an element-by-element basis. Apparent density and the modulus of elasticity were divided into 35 groups, each covering a unique and evenly distributed range of mechanical properties which were mapped onto each element of the meshed bone. The minimum allowed apparent density was 0.01 g/cm^3 (Huiskes and van Rietbergen, 1995, Shultz et al., 2006). The elements which represented the surgically prepared holes had low CT values and thus were assigned a low modulus from this minimum density group. A Poisson's ratio of 0.3 was assigned to all groups.

Yield strain in cancellous bone has been shown to be weakly correlated to density (Kopperdahl and Keaveny, 1998, Kopperdahl et al., 2002) and can be assumed to be uniform within a single anatomical site (Morgan and Keaveny, 2001). Bone was assumed to be elastic-perfectly plastic (Taylor et al., 1995, Silva and Gibson, 1997, Taylor et al., 1998, Silva et al., 1998) with a yield strain of 1.3% (Burgers et al., 2008). The von Mises yield criterion with isotropic hardening was used. The yield stress was calculated for each property group by multiplying the yield strain by the modulus of elasticity of the property group.

The bone was meshed with quadratic tetrahedral elements using a global mesh size of 2.2 mm based on a mesh convergence test. The mesh convergence test was performed for the bone in the bone-implant FE model using the principal strains at the locations of the strain rosettes as feedback.

A node-to-surface, small sliding penalty formulation was used to define the contact conditions in the normal direction of the bone-implant interface. The bone was designated as the "slave" surface and the implant was defined as the "master" surface. The degrees of freedom of the nodes on the slave surface are dependent upon those on the master surface. Frictional contact was defined between the bone and the Ti coating using the penalty method with a static coefficient of friction of 0.5 (Rancourt et al., 1990). The nodes of the CoCr-Ti surface were tied as described previously.

During TKA surgery the implant is impacted onto the femur. This procedure was not simulated in the FE model (Udofia et al., 2007). Instead, the femur was placed so that the intercondylar anterior notch of the implant was centered in the surgically prepared intercondylar anterior notch of the femur (see Figure 7). The geometries of the bone and the implant overlapped, or interfered, in the FE assembly because the AP dimension of the surgically prepared bone was 3-4 mm larger than that of the AP dimension of the implant. The press-fit was resolved in Abaqus by allowing an initial geometrical interference at the beginning of the first step. The interference was gradually removed using a number of increments until the geometries did not overlap. Principal strains were calculated and averaged at each strain rosette location after the interference was resolved.

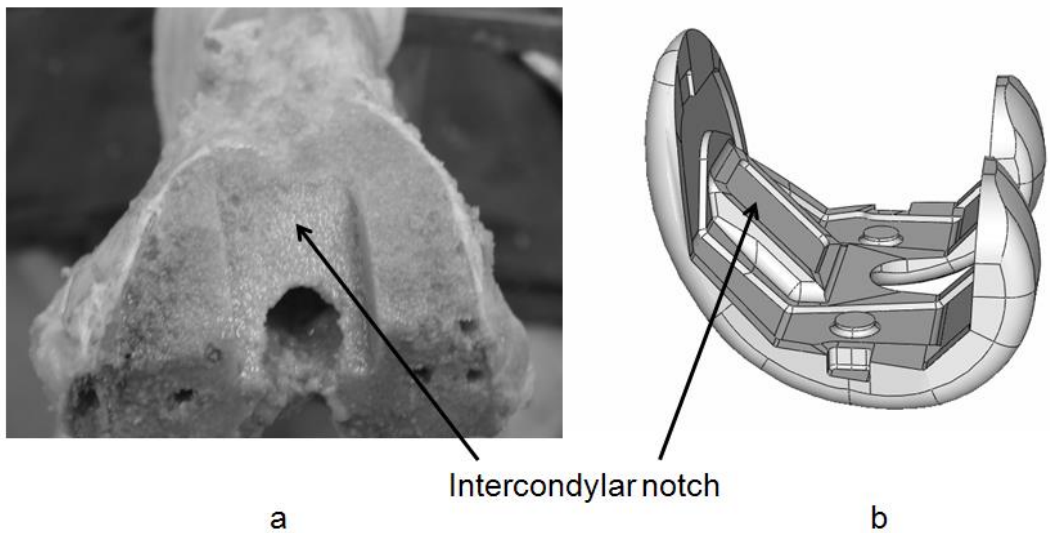

Figure 7 Surgically Prepared Bone and Femoral Component.
a) Photograph of the distal-anterior view of a surgically prepared bone,

b) Sagittal view of a femoral component. The intercondylar notch is identified on each.

The percent difference in the minimum principal strain with respect to the *in vitro* experiment was calculated at each location in the D-1 model. This model was then calibrated with respect to the results of the D-1 *in vitro* experiment by reducing the multiplicative constant in the modulus-density relationship from (2. The modified modulus-density relationship is given in (3. The modified multiplicative constant was chosen to minimize the average of the errors from the four rosette locations in the D-1 model. The modified relationship was used in the D-2 and F-1 models.

$$E = 425\ \rho_{app}^{1.79} \quad (3)$$

3 Results

The strain measurements and predictions from the implant experimental testing and corresponding FE model are shown in Figure 8. The minimum principal strains from the FE model were within 5% of the experiment.

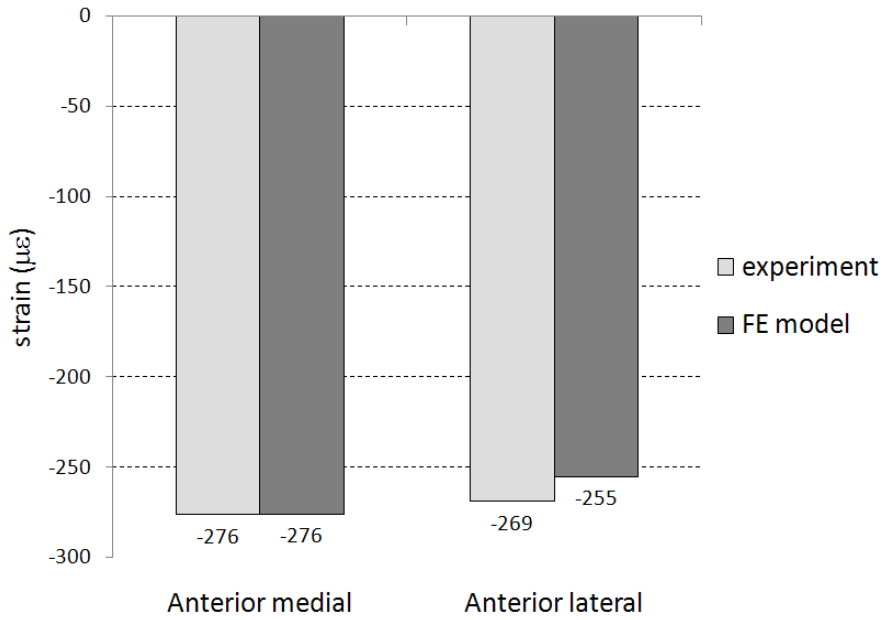

Figure 8 Implant Validation Experimental and FE Minimum Principal Strains.

Minimum principal strains and standard deviations from immediately after implantation for each bone are shown in Figure 9. The magnitude of the strain was larger on the lateral side for both the anterior shield and the posterior condyles for each of the three bones. Figure 10 shows the difference in calculated strains in the D-1 model before and after the modulus of elasticity definition was calibrated. The percent difference values before the modification were between 387 and 863%. The percent difference values after the calibration were -33 to 34%. Figure 11 shows the difference of the minimum principal strains calculated in all of the FE models relative to their *in vitro* measurements using the modulus of elasticity definition as calibrated in the D-1 model. Figure 12 shows the minimum principal strains for the plastic model as previously described and the same model without plasticity (elastic model). The strains are an average of 4.3 times higher in the elastic model.

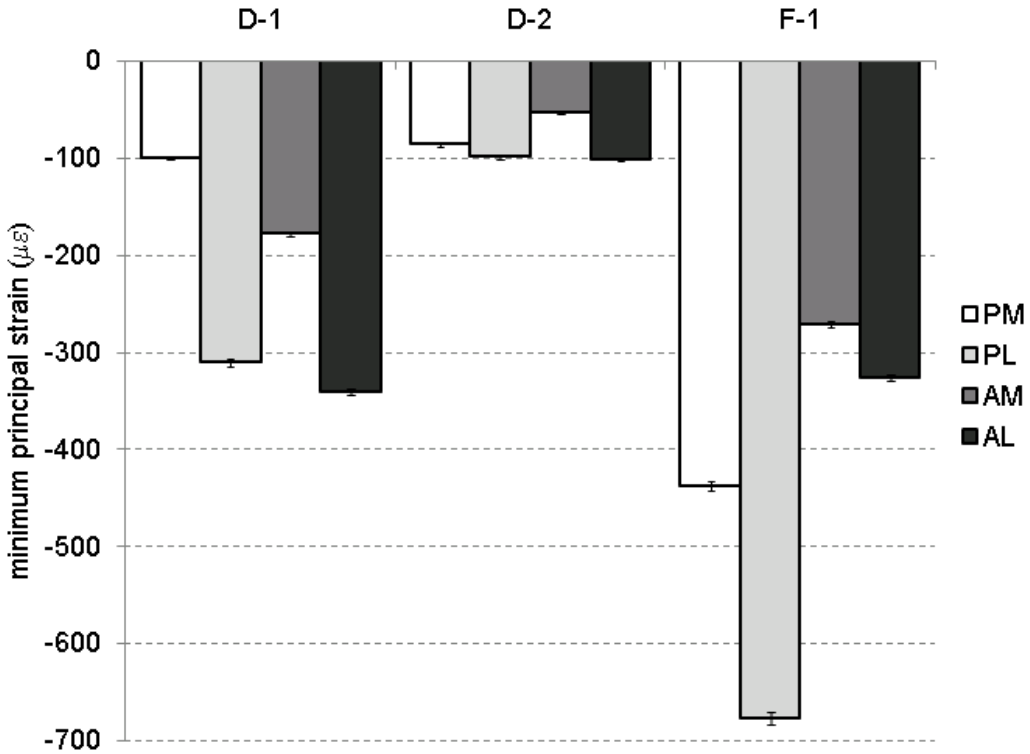

Figure 9 Minimum Principal Strains and Standard Deviations Measured after Implantation. The four strain rosette locations of each component are shown. PM – posterior medial, PL – posterior lateral, AM – anterior medial, AL – anterior lateral.

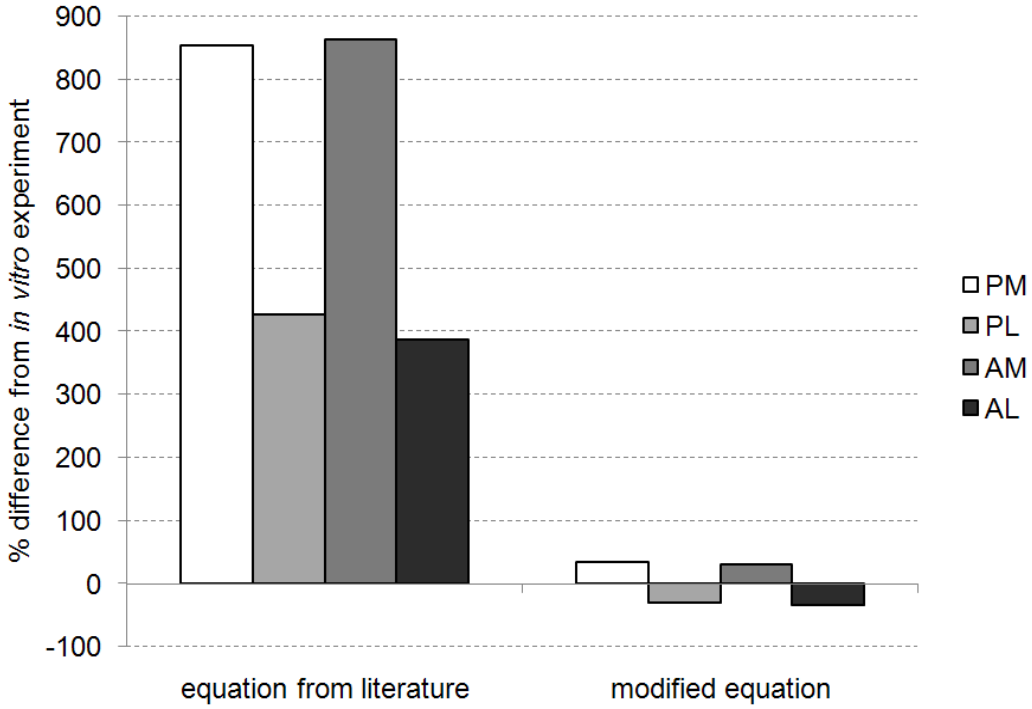

Figure 10 Percent Difference of the Minimum Principal Strains of FE relative to *In Vitro* for Different Modulus of Elasticity Definitions. The D-1 model is shown. PM – posterior medial, PL – posterior lateral, AM –anterior medial, AL – anterior lateral.

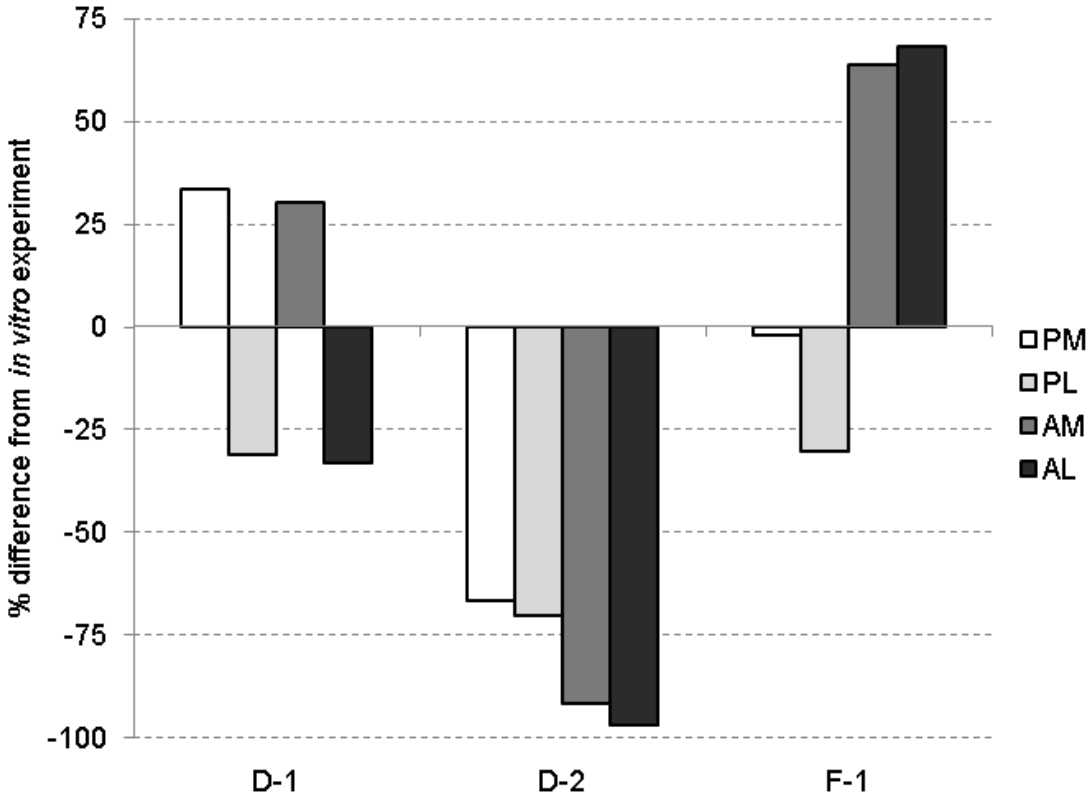

Figure 11 Percent Difference of the Minimum Principal Strains of all the FE Models Relative to their *In Vitro* Results. PM – posterior medial, PL – posterior lateral, AM – anterior medial, AL – anterior lateral.

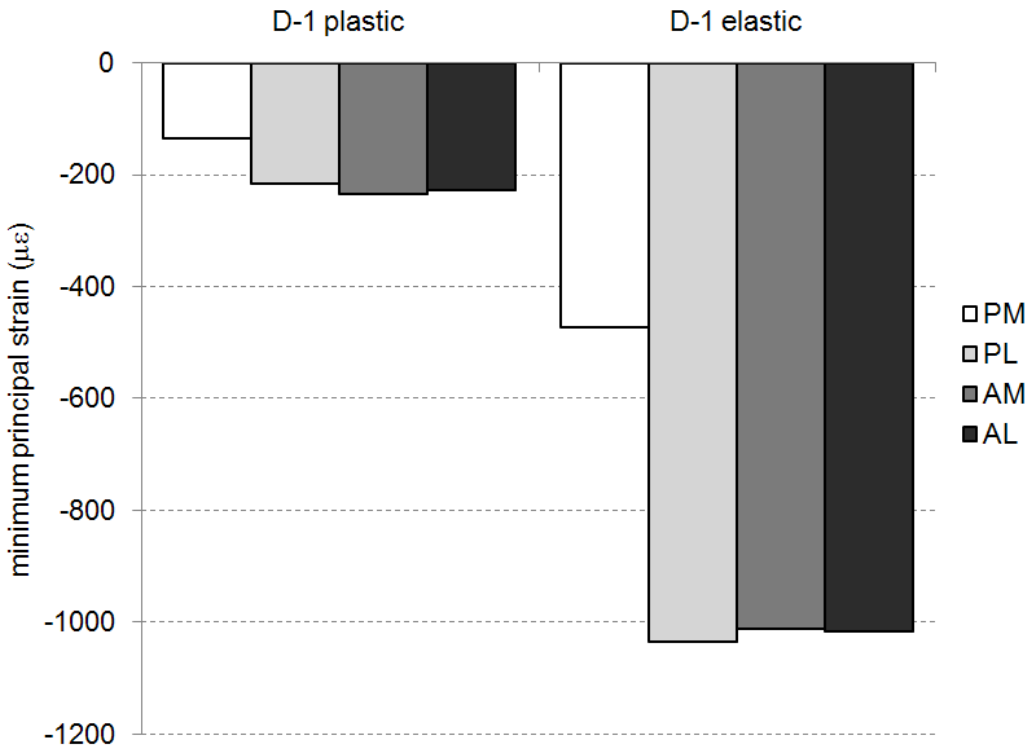

Figure 12 Minimum Principal Strains at the Four Strain Rosette Locations of the D-1 Plastic and Elastic Models. PM – posterior medial, PL – posterior lateral, AM – anterior medial, AL – anterior lateral.

Figure 13 shows the contact pressure calculated from the FE model of each bone. In the contact definition in each model the slave surface (bone) covered more area than that of the master surface (implant). A portion of the excess slave surface was removed in each image for clarity, but some of the surface that was not in contact was included in each image. Thus, there is a darker boundary around the contact area where pressure is mapped but there is no contact. This is clearest in the posterior lateral condyle of the F-1 model where a dark ring surrounds the lighter contact area. The peak pressures were 14.4, 5.0 and 16.5 MPa for the D-1, D-2 and F-1 models, respectively. The peak pressure occurred at a node on the edge of the bone-implant contact surface in each model. The peak occurred at the proximal medial edge of the lateral condyle in the D-1 model, the proximal medial edge of the medial condyle in the D-2 model and the lateral edge of the medial condyle in the F-1 model. The pressure on the posterior condyles was greater than on the anterior shield for each model. In each model the pressure also was generally larger on the lateral

side than the medial. Figure 14 shows the pressures from D-1 using the plastic model and the elastic model. The peak pressure for the D-1 elastic model was ten times (146 MPa) that of the D-1 plastic model and occurred in the same location. The pressures for the elastic model are higher than those in the plastic model. The scale of the elastic pressure map is 5 times larger than the plastic map.

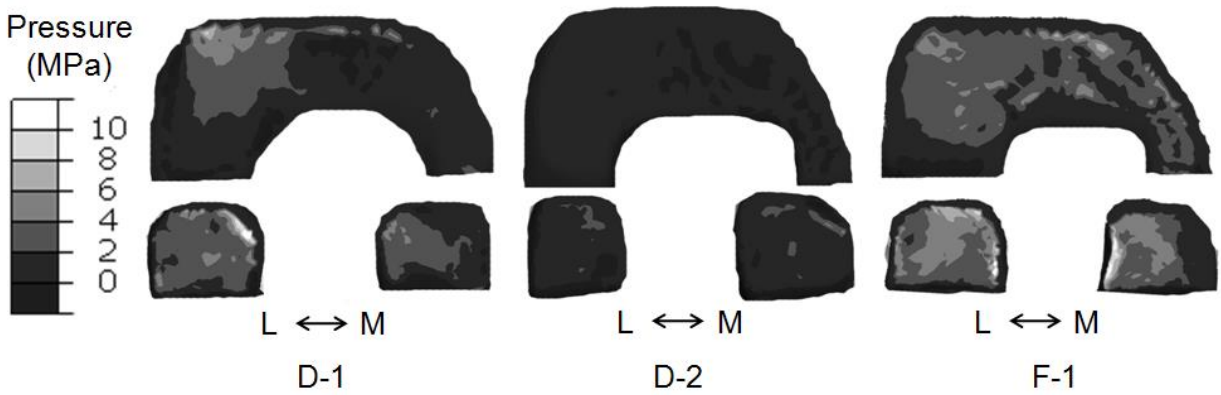

Figure 13 Contact Pressure Map of Bone-Implant Interface Surfaces. Posterior view of anterior shield (see Figure 3b) and posterior condyles (see Figure 3c). M – medial, L – lateral.

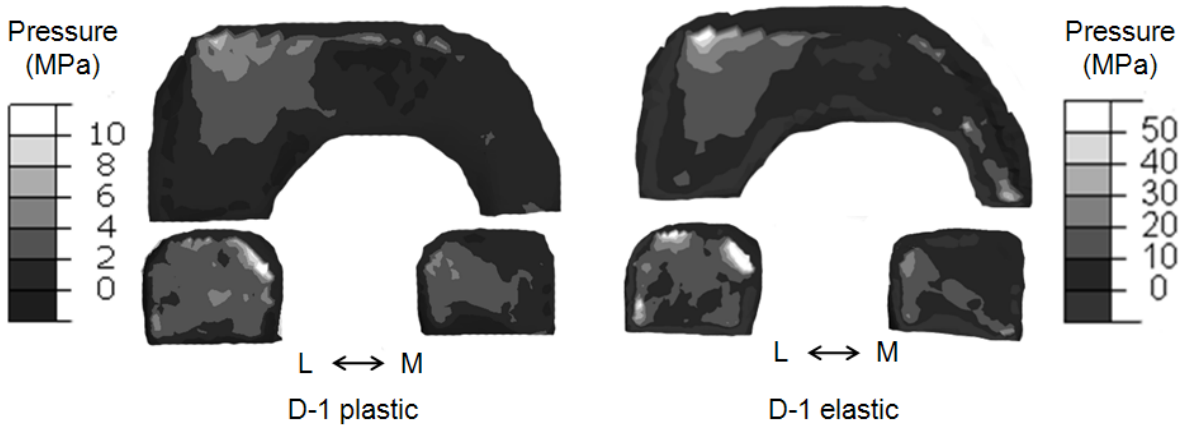

Figure 14 Contact Pressure Map of D-1 Plastic and Elastic Bone-Implant Interface Surfaces. Posterior view of anterior shield (see Figure 3b) and posterior condyles (see Figure 3c). Note the different scales for the plastic and elastic pressures. M – medial, L – lateral.

A large volume of the bone in the box region of the implant experienced plastic strain. Figure 15 shows the plastic strain distribution in four transverse slices of D-1 model. In these images gray elements have some

plastic strain. Much of the lateral side was plastically strained from the proximal edge of the anterior shield to the distal porous coating. The medial side was plastically strained in the distal portion but only had small areas of plastic strain proximal to the proximal edge of the posterior condyles. Figure 16 shows the minimum principal stress trajectories in four transverse slices of D-1 model. The vectors in the stress trajectory plot represent the magnitude and direction of the stress. The stress trajectories are similarly distributed in the medial and lateral sides in the distal slices (c and d) that include the posterior condyles. In the slices that are more superior (a and b) the stress levels are higher in the lateral side than the medial side. Figure 17 shows approximate stress trajectory lines in transverse planes through the proximal and distal ends of the D-1 bone model. In the distal slice, Figure 17b, the lines on both the medial and lateral side are in the general AP direction. In the proximal slice, Figure 17a, the lines on the lateral side are in the general AP direction but the lines on the medial side are directed more at an angle to the AP direction due to the geometry of the implant.

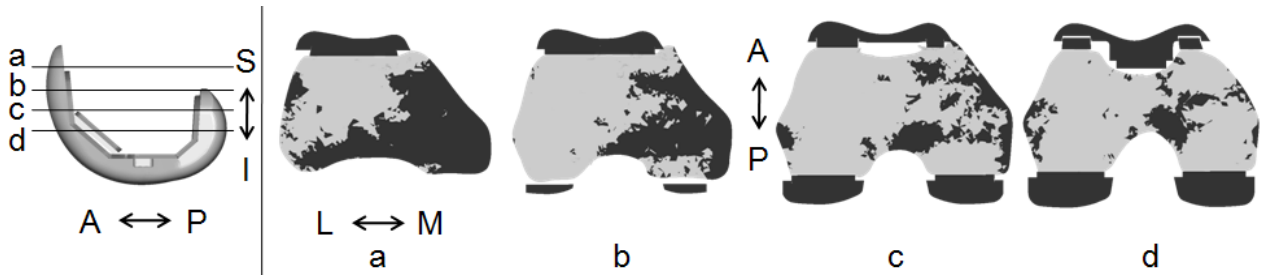

Figure 15 Plastic Regions in the D-1 Bone Shown in the Transverse Plane. Gray elements have plastic strain, black elements do not. Left: Sagittal view of transverse cutting planes, which are described as follows: a) 1 mm proximal to the proximal edge of the anterior shield and 9 mm proximal to the proximal edge of the posterior condyles, b) two thirds of the way up the shield and 2 mm proximal to the proximal edge of the condyles, c) proximal quarter of the condyles and distal third of the shield, d) distal quarter of the condyles and 1 mm distal to the distal end of the shield. M – medial, L – lateral, A – anterior, P – posterior, S – superior, I – inferior.

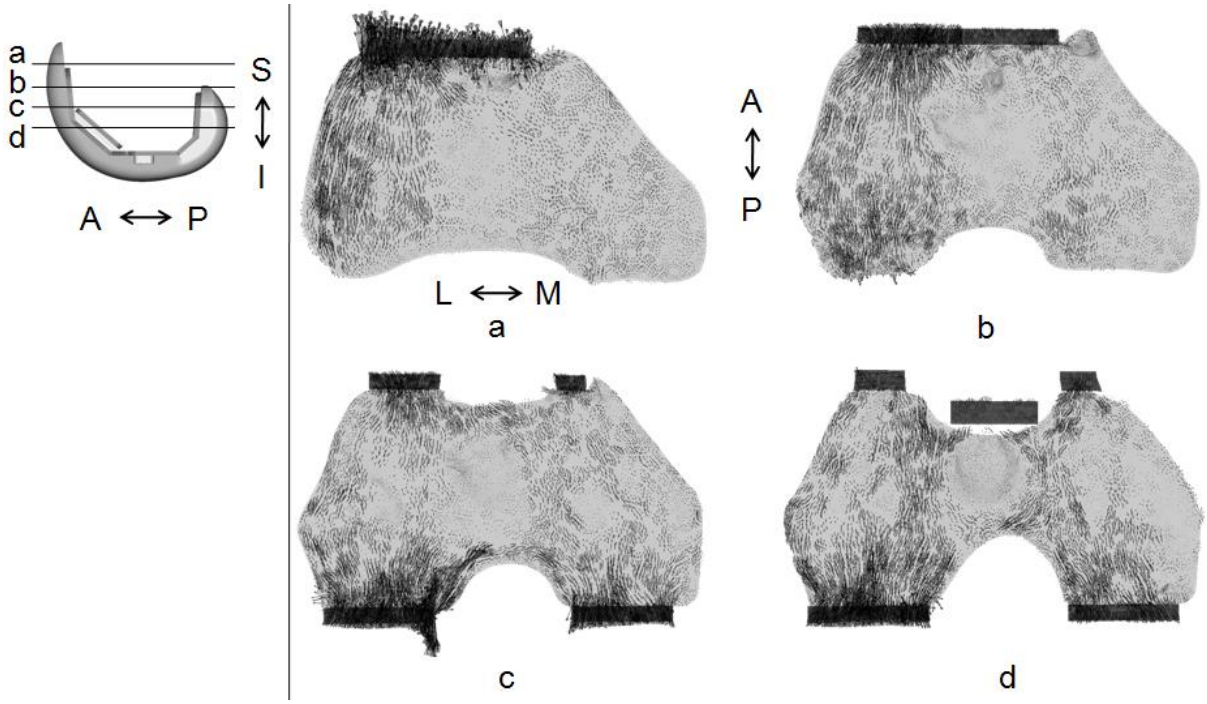

Figure 16 Minimum Principal Stress Trajectories in the D-1 Bone. The transverse plane is shown. Left: Sagittal view of transverse cutting planes, which are described as in Figure 15.

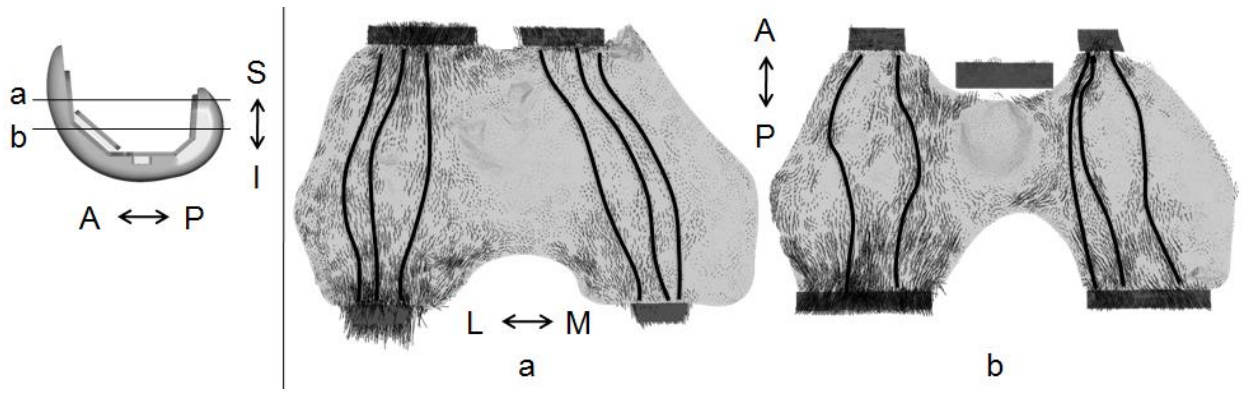

Figure 17 Minimum Principal Stress Trajectories in the D-1 Bone. The transverse plane is shown. Approximate stress flows depicted by solid black lines. Left: Sagittal view of transverse cutting planes, a) distal end and b) proximal end of posterior condyles.

4 Discussion

The minimum principal strains at both strain rosette locations in the F-1 implant FE model were within 5% of the experimentally determined values. This agreement demonstrates that the FE model of the implant with porous coating was accurate to the measured strains for the given load case.

The results of the implant-bone FE models using the equation for elastic modulus versus apparent density from Rho et al. (Rho et al., 1995) in this study produced minimum principal strains of much larger magnitude than the strains measured in the *in vitro* testing. Thus, the equation was modified until the results of one model matched those of the *in vitro* tests of the same bone. The power coefficient in the relationship provided by Rho et al. (1.79) (Rho et al., 1995) is similar to that reported by Ciarelli et al. (1.78) in the AP direction of the distal femur (Ciarelli et al., 1991) and Morgan et al. (1.49-1.93) in the principal trabecular orientation at different anatomical sites (Morgan et al., 2003). Because of this agreement, only the multiplicative coefficient was reduced to calibrate the D-1 FE model. The modified equation ((3) based on (2 and reduced by a factor of 7.7 produced an average error of zero for the minimum principal strains in the four strain rosette locations in the D-1 model. The "modified" modulus of elasticity relationship determined using D-1 model was used in the subsequent FE models: D-2 and F-1.

A longitudinal wave ultrasonic method was used to measure the modulus of elasticity in the study that derived the original equation ((2) for elastic modulus versus apparent density. Ultrasonic methods have been used to determine the elastic mechanical properties of bone by several other authors (Ashman et al., 1987, Ashman et al., 1989, Rho et al., 1993, Rho, 1996, Turner and Eich, 1991, Williams and Johnson, 1989, Nicholson et al., 1997, Kim and Walsh, 1992) as well. A few of these studies have reported the modulus of elasticity of cancellous bone measured using both this ultrasonic technique and mechanical (tension or compression) testing with linear correlations (ratio of ultrasonic to mechanical testing) between the two methods. Ashman et al. reported a linear constant of 1.00 in tensile tests of bovine femoral cancellous bone (Ashman et al., 1987) and the same group (Ashman et al., 1989) reported linear constants of 1.06 and 0.88 in bovine proximal tibia cancellous bone for tension and compression, respectively. Rho et al. found a linear constant of 1.37 in micro-tensile tests of

individual trabeculae (Rho et al., 1993). These results, therefore, do not support the 7.7 reduction factor assumed in the current study.

Besdo et al. used FE models to analyze the method of determining mechanical elastic properties from ultrasonic testing. They stated that the method is acceptable for homogenous materials, as long as the waves are longitudinal. But they warn that the results may be distorted in heterogeneous materials such as cancellous bone (Besdo et al., 2007). Additionally, bone is viscoelastic, and thus strain rate dependent. A higher strain rate used in ultrasonic testing would lead to a stiffer modulus of elasticity than one measured in quasi-static testing (Carter and Hayes, 1976, Carter and Hayes, 1977, Lakes, 1998). Carter and Hayes performed compressive testing on cancellous bone over five decades (10^{-3} to 10 sec^{-1}) of strain rate. They found that the modulus of elasticity (E) was significantly related to apparent density (ρ) and strain rate ($\dot{\varepsilon}$) (Carter and Hayes, 1977, Carter and Hayes, 1976):

$$E = 3790\rho^{3}\dot{\varepsilon}^{0.06} \qquad (4).$$

For a sample tested ultrasonically at 50 kHz (Rho et al., 1995) and quasi-statically at a strain rate of 0.005 sec^{-1} (Keaveny et al., 1994), the estimated ratio of the ultrasonic modulus to the quasi-static modulus using this equation is 3. However, since Carter and Hayes did not test in the ultrasonic frequency range (Carter and Hayes, 1977, Carter and Hayes, 1976) this estimated ratio can only be considered as an initial approximation.

Various other authors have reported that the modulus of elasticity from ultrasonic testing is larger than that from mechanical testing. Williams and Johnson reported a ratio of 2 for bovine tibia cancellous bone (Williams and Johnson, 1989). Kim and Walsh reported a ratio of 3 for bovine femoral cortical bone (Kim and Walsh, 1992). The authors of both of these studies attributed the ratio to the fact that bone is viscoelastic and ultrasonic testing is performed at a higher strain rate than quasi-static mechanical testing. An analysis of the table of data reported by Turner and Eich shows that their results produced a ratio of 23 for bovine cancellous bone from the proximal femur and distal femoral condyles (Turner and Eich, 1991). Nicholson et al. reported a ratio in the superior-inferior direction of 60 for human vertebral cancellous bone (Nicholson et al., 1997). There is a wide range of results in the literature on the relative effect of ultrasonic versus quasi-static material testing; therefore, the 7.7

reduction factor derived in the current study from the *in vitro* test results of specimen D-1 may be justified as a strain rate correction.

The implant-bone FE model for specimen D-1 using the "modified" modulus-density relationship produced minimum principal strains between -33 and 34% compared to the *in vitro* results. This range in percent difference between the calibrated model and *in vitro* results is expected considering the large variations inherent to *in vitro* testing on cadaveric specimens. As discussed above, the ratio of the ultrasonic to quasi-static methods has been shown to vary between 1 and 60. The accuracy of the D-2 and F-1 models using the same "modified" relationship should be considered with respect to these calibration limits. The differences in the minimum principal strains in the F-1 model, with respect to the *in vitro* implantation, were 2-68%. The D-2 specimen had the lowest density bone and its FE model under-predicted the minimum principal strains by 67-97%. The under-prediction of the strains in D-2 specimen may be due to the fact that the modulus-density relations were determined for non-osteoporotic bone. It is possible that the low density bone was osteoporotic and that the elastic modulus versus apparent density relationships derived from healthy bone do not apply.

The pressure at the bone-implant interfaces can be qualitatively compared to the minimum principal strains measured at the strain rosette locations during *in vitro* implantation. The rank order of the pressures on the surfaces and the minimum principal strains were, from highest to lowest, F-1, D-1 and D-2. As the bone-implant interface pressure increases, the frictional force will also increase; therefore, the primary fixation strength is also expected to improve with increased interface pressures. This direct relationship between the implant strain at the rosette locations and primary fixation strength demonstrates that it is possible to make relative comparisons of bone-implant fixation strength by monitoring the strain on the external face of the femoral knee component. Strain rosette locations affect the strain results so care must be taken in determining the locations of the rosettes when comparing the results of different sized implants, especially if *in vitro* testing is performed without FE analyses.

Bellini et al. (Bellini et al., 2007) and Udofia et al. (Udofia et al., 2007) presented pressure maps of press-fit acetabular components using FE models, but warned that results should be used qualitatively. Bellini et al. created an FE model with a linear-elastic, heterogeneous bone property definition to investigate a 54 mm diameter acetabular cup implanted with

a diametrical interference of 2 mm. They reported bone-implant interface peak pressures occurred around the rim of an acetabular component (8-10 MPa with a peak of 20 MPa). The minimum pressure (1 MPa) on the interface was determined at the pole of the cup (Bellini et al., 2007). Udofia et al. reported results from an FE model with a linear-elastic, homogeneous bone property definition for a 50 mm diameter acetabular cup implanted with diametrical interferences of 1 and 2 mm. They also reported peak pressures around the rim of the cup (generally less than 16 MPa and 30 MPa with peak pressures of 24.3 MPa and 53.6 MPa, for each of the interferences, respectively). The minimum pressures (less than 3 MPa) were found at the pole of the cup (Udofia et al., 2007). In contrast to the current study, the mechanical property definitions in both of these studies were linear elastic. Bellini et al. stated that adding plasticity would likely decrease the contact pressures, which might account for the lower bone-implant interface pressures found in the current study (Bellini et al., 2007). The results of the current study agree with this assessment, as the pressure reported here was in general about five times greater in the D-1 elastic model compared to the plastic model. It is clear that plasticity had a large effect on the results of the model and needs to be considered for this press-fit condition. The peak pressures of the plastic models reported in the current study (Figure 13) occurred at the boundary of the bone-implant interface. This is consistent with the two studies described on acetabular components (Udofia et al., 2007, Bellini et al., 2007) and the analytical solution for a cylindrical indenter on a semi-infinite solid (Timoshenko and Goodier, 1951).

The press-fit interface of the femoral knee component is caused by the interfering geometry of the distal femur and the implant. Specifically, the bone is surgically cut so that it has a larger AP dimension than the implant. The degree of initial fixation is a function of both the geometry and the density of the bone. The higher the density of the bone, the higher the press-fit forces and the stronger the primary fixation of the implant will be. This was demonstrated by increased pressure and a larger magnitude of minimum principal strains at the rosette locations. The rank order of the minimum principal strains at the four rosette locations and pressures was the same as the rank order of the density: F-1, D-1 and D-2. The FE models successfully predicted the rank order of the density of and the primary fixation for the three bones.

This study is the first to show that cancellous bone in the distal femur yields after implantation of a femoral knee component. Taylor et al.

(Taylor et al., 1998) found selected regions under a tibial component yielded but the regions were not as large as was determined in the FE models presented here. This finding provides reason to investigate the post-yield behavior of cancellous bone. It would be especially interesting to analyze post-yield remodeling because of the osseointegration that occurs in a press-fit femoral component.

Figure 15 shows that most of the elements in both the medial and lateral sides of the bone in the distal slices (c and d) have yielded. In the proximal slices (a and b) the lateral side had many more elements that yielded than the medial. Figure 17 shows how the minimum principal stress trajectories decreased in the more proximal regions of the bone. The geometry of the implant and its alignment on the bone caused the bone in the proximal medial region to remain elastic while the lateral was plastic. Because of the 3° external rotation of the component on femur, the medial side of the shield was more lateral than the medial condyle, as is clear in Figure 17a. This offset also caused a moment and corresponding rotation in the medial compartment. Since the shield was more lateral than the condyle, the bone was not able to be compressed in the same way as the geometry dictates on the lateral side. The fact that the lateral shield and condyle were more aligned in the press-fit (AP) direction also caused higher stresses and bone-implant pressures on the lateral side than the medial (see Figure 13). The higher pressures on the lateral side correspond to larger magnitude of strains measured on the lateral side. This is more apparent in the posterior condyles than the anterior shield (see Figure 9) because the strain rosettes on the posterior condyles are independent of one another while the rosettes on the anterior shield are not. A pressure anywhere on the shield will cause strains in both rosettes on the shield.

One limitation of this study is that the FE models cannot be used to predict bone fracture because a fracture criterion for bone was not included. For example, keeping all other conditions the same, the bone would fix better to the implant with a larger AP dimension, but there is a limit to this physical dimension, as the bone could fracture if it must compress too much to fit in the implant. The FE models included a yield strain limit that is independent of density (Morgan and Keaveny, 2001), but this assumption may not hold for pathological bone. If the yield strain increased with increasing apparent density, lower density pathological bone would have a lower yield strain. This would lead to a lower maximum stress in the bone and weaker fixation strength.

The intent of this study was to focus on the initial fixation of the bone-implant interface. Under physiological loading, the pressure on the surfaces is expected to change from the initial fixation condition discussed. The pressure under these loading conditions will affect the micromotion and therefore osseointegration (Pilliar et al., 1986, Jasty et al., 1997) and long-term fixation of the knee component.

A previous study that included FE models and experimental testing of a femoral knee component has been performed on synthetic bone (Completo et al., 2007), but the current study is the first to analyze primary fixation of a press-fit femoral knee component using the combination of *in vitro* testing and FE analysis. Specifically, this study was the first to include the combination of *in vitro* implantation and subject-specific, calibrated FE models of the distal femur-femoral knee component interface. This is an important combination that could be used to preoperatively assess primary fixation and potentially reduce the occurrence of femoral component loosening.

5 Conclusions

Initial fixation of a femoral knee component was successfully predicted *in vitro* using strain rosettes on the external surface of the implant. This method can be used to qualitatively assess relative fixation. Subject-specific FE models were successfully created and calibrated from the *in vitro* experiment. The implant and porous coating used in these models were validated against experimental testing of strain gauged implants. The implementation of plasticity in bone of the FE models decreased the fixation strength considerably from a purely elastic FE model.

The initial fixation of the femoral knee component was related to the geometry of the surgical cuts and the density of the bone. The initial fixation, demonstrated by the minimum principal strain at the rosette locations and the pressure on the internal surfaces, increased with bone density. The geometry of the surgical cuts and the femoral component caused the cancellous bone to deform plastically.

In the current study, the geometry and alignment of the implant resulted in higher stresses and pressures on the lateral side than the medial side, especially proximal to the posterior condyles. The medial bone in this region was therefore not plastically strained to the same extent as the lateral side.

6 Conflict of Interest Statement

Dr. Mason is an employee of Zimmer Inc., manufacturer of the NexGen implant system.

7 Acknowledgements

T. Burgers gratefully acknowledges the support of Zimmer, Inc. for this study. The authors also acknowledge Eric Graves for attaching the strain rosettes, Geoff Pillar for assistance during the implant validation testing, Danny Levine for assistance creating the FE model, and Dr. Matthew Squire and Juan Vivanco for their insight.

8 References

ASHMAN, R. B., CORIN, J. D. & TURNER, C. H. (1987) Elastic properties of cancellous bone: measurement by an ultrasonic technique. *Journal of Biomechanics,* 20**,** 979-86.

ASHMAN, R. B., RHO, J. Y. & TURNER, C. H. (1989) Anatomical variation of orthotropic elastic moduli of the proximal human tibia. *Journal of Biomechanics,* 22**,** 895-900.

BARINK, M., VERDONSCHOT, N. & DE WAAL MALEFIJT, M. (2003) A different fixation of the femoral component in total knee arthroplasty may lead to preservation of femoral bone stock. *Proceedings of The Institution of Mechanical Engineers Part H, Journal of Engineering In Medicine,* 217**,** 325-32.

BELLINI, C. M., GALBUSERA, F., CERONI, R. G. & RAIMONDI, M. T. (2007) Loss in mechanical contact of cementless acetabular prostheses due to post-operative weight bearing: a biomechanical model. *Medical Engineering & Physics,* 29**,** 175-81.

BESDO, D., BESDO, S., BEHRENS, B. A. & BOUGUECHA, A. (2007) Problems with ultrasonic measurements of shear modules of structured media. *Acta Biomaterialia,* 3**,** 723-33.

BURGERS, T. A., MASON, J., NIEBUR, G. & PLOEG, H. L. (2008) Compressive properties of trabecular bone in the distal femur. *Journal of Biomechanics,* 41**,** 1077-85.

CARTER, D. R. & HAYES, W. C. (1976) Bone Compressive Strength - Influence of Density and Strain Rate. *Science,* 194**,** 1174-1176.

CARTER, D. R. & HAYES, W. C. (1977) The compressive behavior of bone as a two-phase porous structure. *Journal of Bone and Joint Surgery American Volume,* 59**,** 954-62.

CHOCKALINGAM, S. & SCOTT, G. (2000) The outcome of cemented vs. cementless fixation of a femoral component in total knee replacement (TKR) with the identification of radiological signs for the prediction of failure. *Knee,* 7**,** 233-238.

CIARELLI, M. J., GOLDSTEIN, S. A., KUHN, J. L., CODY, D. D. & BROWN, M. B. (1991) Evaluation of orthogonal mechanical properties and density of human trabecular bone from the major metaphyseal regions with materials testing and computed tomography. *Journal of Orthopaedic Research,* 9**,** 674-82.

COMPLETO, A., FONSECA, F. & SIMOES, J. A. (2007) Experimental validation of intact and implanted distal femur finite element models. *Journal of Biomechanics,* 40**,** 2467-76.

DEFRANCES, C. J., CULLEN, K. A. & KOZAK, L. J. (2007) National Hospital Discharge Survey: 2005 annual summary with detailed

diagnosis and procedure data. *Vital and Health Statistics Series 13, Data From The National Health Survey*, 1-209.

EUROPE INFORMATION SOCIETY (2007) DESSOS: Decision Support Software for Orthopaedic Surgery.

HAAS, S. B., INSALL, J. N., MONTGOMERY, W., 3RD & WINDSOR, R. E. (1995) Revision total knee arthroplasty with use of modular components with stems inserted without cement. *Journal of Bone and Joint Surgery American Volume,* 77**,** 1700-7.

HUISKES, R. & VAN RIETBERGEN, B. (1995) Preclinical testing of total hip stems. The effects of coating placement. *Clinical Orthopaedics and Related Research***,** 64-76.

JASTY, M., BRAGDON, C., BURKE, D., O'CONNOR, D., LOWENSTEIN, J. & HARRIS, W. H. (1997) In vivo skeletal responses to porous-surfaced implants subjected to small induced motions. *Journal of Bone and Joint Surgery American Volume,* 79**,** 707-14.

KEAVENY, T. M., GUO, X. E., WACHTEL, E. F., MCMAHON, T. A. & HAYES, W. C. (1994) Trabecular bone exhibits fully linear elastic behavior and yields at low strains. *Journal of Biomechanics,* 27**,** 1127-36.

KIM, H. D. & WALSH, W. R. (1992) Mechanical and ultrasonic characterization of cortical bone. *Biomimetics,* 1**,** 293-310.

KING, T. V. & SCOTT, R. D. (1985) Femoral component loosening in total knee arthroplasty. *Clinical Orthopaedics and Related Research***,** 285-90.

KOPPERDAHL, D. L. & KEAVENY, T. M. (1998) Yield strain behavior of trabecular bone. *Journal of Biomechanics,* 31**,** 601-8.

KOPPERDAHL, D. L., MORGAN, E. F. & KEAVENY, T. M. (2002) Quantitative computed tomography estimates of the mechanical properties of human vertebral trabecular bone. *Journal of Orthopaedic Research,* 20**,** 801-805.

LAKES, R. S. (1998) *Viscoelastic Solids,* Boca Raton, FL, CRC Press.

MALONEY, W. J., JASTY, M., BURKE, D. W., O'CONNOR, D. O., ZALENSKI, E. B., BRAGDON, C. & HARRIS, W. H. (1989) Biomechanical and histologic investigation of cemented total hip arthroplasties. A study of autopsy-retrieved femurs after in vivo cycling. *Clinical Orthopaedics and Related Research***,** 129-40.

MORGAN, E. F., BAYRAKTAR, H. H. & KEAVENY, T. M. (2003) Trabecular bone modulus-density relationships depend on anatomic site. *Journal of Biomechanics,* 36**,** 897-904.

MORGAN, E. F. & KEAVENY, T. M. (2001) Dependence of yield strain of human trabecular bone on anatomic site. *Journal of Biomechanics,* 34**,** 569-77.

NICHOLSON, P. H., CHENG, X. G., LOWET, G., BOONEN, S., DAVIE, M. W., DEQUEKER, J. & VAN DER PERRE, G. (1997) Structural and material mechanical properties of human vertebral cancellous bone. *Medical Engineering & Physics,* 19**,** 729-37.

PHILLIPS, T. W., MESSIEH, S. S. & MCDONALD, P. D. (1990) Femoral stem fixation in hip replacement. A biomechanical comparison of cementless and cemented prostheses. *Journal of Bone and Joint Surgery British Volume,* 72**,** 431-4.

PILLIAR, R. M., LEE, J. M. & MANIATOPOULOS, C. (1986) Observations on the effect of movement on bone ingrowth into porous-surfaced implants. *Clinical Orthopaedics and Related Research***,** 108-13.

RANCOURT, D., SHIRAZI-ADL, A., DROUIN, G. & PAIEMENT, G. (1990) Friction properties of the interface between porous-surfaced metals and tibial cancellous bone. *Journal of Biomedical Materials Research,* 24**,** 1503-19.

REGGIANI, B., CRISTOFOLINI, L., VARINI, E. & VICECONTI, M. (2007) Predicting the subject-specific primary stability of cementless implants during pre-operative planning: preliminary validation of subject-specific finite-element models. *Journal of Biomechanics,* 40**,** 2552-8.

RHO, J. Y. (1996) An ultrasonic method for measuring the elastic properties of human tibial cortical and cancellous bone. *Ultrasonics,* 34**,** 777-83.

RHO, J. Y., ASHMAN, R. B. & TURNER, C. H. (1993) Young's modulus of trabecular and cortical bone material: ultrasonic and microtensile measurements. *Journal of Biomechanics,* 26**,** 111-9.

RHO, J. Y., HOBATHO, M. C. & ASHMAN, R. B. (1995) Relations of mechanical properties to density and CT numbers in human bone. *Medical Engineering & Physics,* 17**,** 347-355.

ROBERTSSON, O., KNUTSON, K., LEWOLD, S. & LIDGREN, L. (2001) The Swedish Knee Arthroplasty Register 1975-1997: an update with special emphasis on 41,223 knees operated on in 1988-1997. *Acta Orthopaedica Scandinavica,* 72**,** 503-13.

SHARKEY, P. F., HOZACK, W. J., ROTHMAN, R. H., SHASTRI, S. & JACOBY, S. M. (2002) Why are total knee arthroplasties failing today? (Insall Award paper). *Clinical Orthopaedics and Related Research***,** 7-13.

SHULTZ, T. R., BLAHA, J. D., GRUEN, T. A. & NORMAN, T. L. (2006) Cortical bone viscoelasticity and fixation strength of press-fit femoral stems: finite element model. *Journal of Biomechanical Engineering,* 128**,** 7-12.

SILVA, M. J. & GIBSON, L. J. (1997) Modeling the mechanical behavior of vertebral trabecular bone: effects of age-related changes in microstructure. *Bone,* 21**,** 191-9.

SILVA, M. J., KEAVENY, T. M. & HAYES, W. C. (1998) Computed tomography-based finite element analysis predicts failure loads and fracture patterns for vertebral sections. *Journal of Orthopaedic Research,* 16**,** 300-8.

TAYLOR, M., TANNER, K. E. & FREEMAN, M. A. (1998) Finite element analysis of the implanted proximal tibia: a relationship between the initial cancellous bone stresses and implant migration. *Journal of Biomechanics,* 31**,** 303-10.

TAYLOR, M., TANNER, K. E., FREEMAN, M. A. R. & YETTRAM, A. L. (1995) Finite element modelling—predictor of implant survival? *Journal of materials science. Materials in medicine,* 6**,** 808-812.

TIMOSHENKO, S. P. & GOODIER, J. N. (1951) *Theory of elasticity,* New York, McGraw-Hill.

TISSAKHT, M., AHMED, A. M. & CHAN, K. C. (1996) Calculated stress-shielding in the distal femur after total knee replacement corresponds to the reported location of bone loss. *Journal of Orthopaedic Research,* 14**,** 778-85.

TURNER, C. H. & EICH, M. (1991) Ultrasonic velocity as a predictor of strength in bovine cancellous bone. *Calcified Tissue International,* 49**,** 116-9.

UDOFIA, I., LIU, F., JIN, Z., ROBERTS, P. & GRIGORIS, P. (2007) The initial stability and contact mechanics of a press-fit resurfacing arthroplasty of the hip. *Journal of Bone and Joint Surgery British Volume,* 89**,** 549-56.

VAN LENTHE, G., WILLEMS, M., VERDONSCHOT, N., DE WAAL MALEFIJT, M. & HUISKES, R. (2002) Stemmed femoral knee prostheses: effects of prosthetic design and fixation on bone loss. *Acta Orthopaedica Scandinavica,* 73**,** 630-7.

VAN LENTHE, G. H., DE WAAL MALEFIJT, M. C. & HUISKES, R. (1997) Stress shielding after total knee replacement may cause bone resorption in the distal femur. *Journal of Bone and Joint Surgery British Volume,* 79**,** 117-22.

VICECONTI, M., MUCCINI, R., BERNAKIEWICZ, M., BALEANI, M. & CRISTOFOLINI, L. (2000) Large-sliding contact elements

accurately predict levels of bone-implant micromotion relevant to osseointegration. *Journal of Biomechanics,* 33**,** 1611-8.

WILLIAMS, J. L. & JOHNSON, W. J. (1989) Elastic constants of composites formed from PMMA bone cement and anisotropic bovine tibial cancellous bone. *Journal of Biomechanics,* 22**,** 673-82.